MATHEMATICAL AND COMPUTER MODELLING OF DYNAMICAL SYSTEMS
https://doi.org/10.1080/13873954.2020.1786841

Taylor & Francis
Taylor & Francis Group

ARTICLE

Fluid-Structure Port-Hamiltonian Model for Incompressible Flows in Tubes with Time Varying Geometries

Luis A. Mora[a,b], Le Gorrec Yann[a], Hector Ramirez[b] and Juan Yuz[b]

[a]Univ. Bourgogne Franche-Comté, Univ. De Franche-Comté/ENSMM, Besançon, France; [b]Advanced Center for Electrical and Electronic Engineering, Universidad Técnica Federico Santa María, Valparaiso, Chile

ABSTRACT

A simple and scalable finite-dimensional model based on the port-Hamiltonian framework is proposed to describe the fluid–structure interaction in tubes with time-varying geometries. For this purpose, the moving tube wall is described by a set of mass-spring-damper systems while the fluid is considered as a one-dimensional incompressible flow described by the average momentum dynamics in a set of incompressible flow sections. To couple these flow sections small compressible volumes are defined to describe the pressure between two adjacent fluid sections. The fluid-structure coupling is done through a power-preserving interconnection between velocities and forces. The resultant model includes external inputs for the fluid and inputs for external forces over the mechanical part that can be used for control or interconnection purposes. Numerical examples show the accordance of this simplified model with finite-element models reported in the literature.

ARTICLE HISTORY
Received 24 January 2020
Accepted 21 June 2020

KEYWORDS
Port-Hamiltonian systems; Fluid-structure interactions; incompressible fluids; scalable finite-dimensional model

1. Introduction

Fluid–structure interaction (FSI) stems from the reciprocal action between an elastic structure and a fluid flow through a contact surface [1]. In this work, we consider an incompressible flow in tubes with time-varying geometries, as shown in Figure 1. This FSI problem plays an important role in several applications, such as the study of the blood flow in vessels [2–4] and the human phono-respiratory system [5–9], among others.

From a numerical point of view, FSI problems have some drawback, such as; they require an appropriate grid for the mechanical and fluid domains, a clear delineation of fluid–structure interface [10], an appropriate estimation of the nonlinear dynamics, and the numerical stability of the discretization methods. In the literature, different approaches have been proposed to solve these drawbacks. For example, in [11] a generic form of fluid governing equations is used in an Arbitrary Lagrangian-Eulerian (ALE) frame and the nonlinear generalized-α time integration scheme is used to estimate the flow dynamics. In [12] the flow is described through a linear incompressible inviscid model in an ALE formulation and the mechanical movement is given by a generalized string model, using

CONTACT Luis A. Mora luis.moraa@sansano.usm.cl FEMTO-ST Institute, AS2M Department, Univ. Bourgogne Franche-Comté, Univ. De Franche-Comté/ENSMM, BesanÃ§on F-25000, France

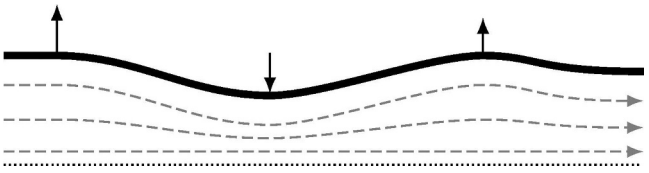

Figure 1. Incompressible flow in a tube with time-varying geometry. The solid line represents the tube walls and the arrows represent the magnitude and sense of wall velocity at corresponding points. Dashed lines are the flow streamlines.

a Leap Frog-Implicit Euler time discretization scheme. Similarly, in [4] an axisymmetric Navier-Stokes Prandtl (RNS-P) system is used and the fluid-structure dynamics are obtained using a finite volume "multiring" algorithm. With respect to the numerical stability, it is common to use an energy-based analysis, i.e. the conservation of the energy balance by the discretization algorithms, as shown in [3,13].

Another problem related to incompressible fluids is the causality of the pressure in the numerically discretized momentum equation. In this sense, pressure-pressure coupling algorithms are commonly used, such as, for example, backward approximation pressure-correction schemes [14] and pseudo-compressible algorithms, such as the Petrov–Galerkin method [15].

In this work, we simplify the mechanical dynamics using a set of mass-spring-damper systems to describe the wall movement. Furthermore, we consider the fluid as a one-dimensional incompressible flow described by the average momentum dynamics in a set of incompressible flow sections. To solve the causality problem on the pressure we use and expand the approach proposed in [16], defining small compressible volumes, called nodes, where small variations in the density are used to describe the pressure between two adjacent incompressible fluid sections, allowing consistent coupling between two incompressible fluid sections.

The aim of this work is to propose a simple, scalable and energy-consistent model for the continuous dynamic behaviour of flows in tubes with time-varying geometries. To this purpose, we use the port-Hamiltonian systems (PHS) framework that is particularly suited for the modelling of continuous nonlinear systems. PHS framework has been used to describe compressible flows [17–19], magnetohydrodynamics [20] and to study the FSI of liquid sloshing in moving containers [21]. In the PHS framework, the dynamics are associated with a non-negative potential function that represents the systems total energy and an inner product as well as input and output signals representing the power supplied to the system. As a consequence, two PHS for different physical domains can be interconnected through their ports, whose product represents the power exchange between both systems. Therefore, the port-Hamiltonian formulation is a useful tool to describe multi-physical problems. Another advantage of PHS is that they guarantee properties for control, such as passivity and stability [22,23]. Additionally, PHS generates a Dirac structure [23], allowing the use of mathematical tools, like Lie algebra [24], to analyse the system properties.

In this work, we use the port-Hamiltonian framework to derive a scalable finite-dimensional model of an incompressible flow in a tube with time-varying geometries. Incompressible sections and nodes in the fluid are used as kinetic and potential storage

elements, respectively, to obtain a PHS formulation that is coupled with the mechanical model of the structure using a power-preserving interconnection.

The remainder of the paper is organized as follows: In Section 2 we give a description of the system and the assumptions considered for the model. In Sections 3 and 4 we develop the mechanical and fluid models, respectively. In Section 5 we describe the interconnection between the two systems to get the overall model. Finally, in Section 6 numerical examples are given, and Section 7 presents the conclusions. Additionally, a notation table is included in the Appendix.

2. System description

In this work, we consider an incompressible fluid in a tube of which the wall is moving. This movement is influenced by the force exerted by the fluid flow and some possible external forces. At the same time, the flow dynamics are affected by boundary conditions, that changes according to the wall movement. We consider a symmetrical behaviour of the fluid and wall dynamics, hence, the fluid description is reduced to a 2D incompressible flow. We use a modular modelling approach to describe the wall and flow dynamics in a number of tube sections used as lumped elements that are coupled.

In this end, we use a set of interconnected mass-spring-damper (MSD) systems to characterize the moving wall, as shown in Figure 2. In this figure, each dotted box is an MSD system that describes the motion of one tube section.

In this work, the fluid dynamics are described by the well-known continuity and motion equations [25], in their incompressible form and neglecting the gravitational effects, leading to

$$\cdot(\mathbf{v}) = 0 \tag{1}$$

$$\rho\partial_t\mathbf{v} + \rho\mathbf{v}\cdot \quad \mathbf{v} + \quad p = \mu \quad ^2\mathbf{v} \tag{2}$$

where ρ, $\mathbf{v}$, p and μ are the density, velocity field, pressure and viscosity of the fluid flow, respectively, $\cdot()$, and ^{2} describes the divergence, gradient and Laplacian operators, respectively, and $\partial_t = \frac{\partial}{\partial t}$.

Notice that (1) is, from a mathematical point of view, the approximation of the more general mass balance $\partial_t\rho + \quad \cdot(\rho\mathbf{v}) = 0$, when we assume that the variations of the fluid density are negligible, i.e. $\Delta\rho \lll \rho$. We use the Mach number (M) to

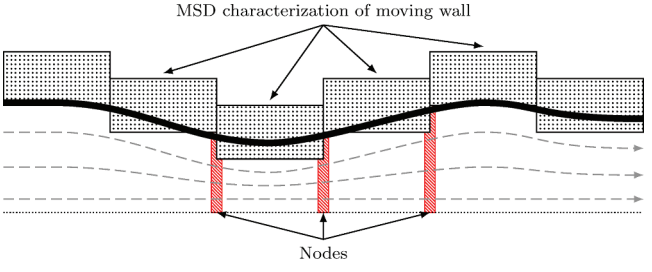

Figure 2. Mechanical description of wall movement. Each box dotted represent one MSD system.

consider when this incompressibility assumption is adequate. In this work we study flows with $M \leq 0.3$ [26]. In different studies on incompressible flows, it is common to use pseudo-compressible algorithms, such as the Pretrov–Galerkin method, to define appropriate pressure-pressure couplings [15] in the space discretization of (2). Similarly, in this work, we relax the incompressible hypothesis to describe the pressure in different zones of the fluid domain. The considered moving wall characterization implies that the flow channel presents sudden expansions and contractions. Additionally, we can reduce the fluid analysis to a 1D incompressible flow, as shown in Section 4. Thus, we divide the fluid domain into sections with uniform cross-sectional area where the flow is incompressible to describe the fluid dynamics and infinitesimal compressible sections, that will be denoted by nodes to describe the pressure in the coupling zone between two adjacent incompressible sections, as shown in Figure 2. The use of nodes to couple incompressible sections has been applied in [16] for tubes with fixed irregular geometries. In this work, we extend this idea to consider time-varying geometries. We define the fluid behaviour in nodes using the following assumption.

Assumption 1. *The volume of a node i is small enough, such that the density distribution is uniform, and the changes in density are only caused by changes in the volume [27, Sec. 5.1,* p.78]. *This implies that the mass in each node is constant, i.e. the following relationship is satisfied*

$$\rho_i \bar{V}_i = \kappa \tag{3}$$

where ρ_i and $\bar{V}_i$ are the density and volume of the i-th node, and κ is the node total mass.

As mentioned above, we use the PHS framework to describe the ODEs associated with the wall and fluid dynamics. In this sense, according to [22,23] an input-state-output PHS with direct feed-through is given by

$$\underline{\mathbf{x}} = (J - R)\partial_{\mathbf{x}} H + (g - P)\mathbf{u} \tag{4a}$$

$$\mathbf{y} = (g + P)^T \partial_{\mathbf{x}} H + (M + S)\mathbf{u} \tag{4b}$$

where $\mathbf{x}$ is the state vector, $(\mathbf{u}, \mathbf{y})$ are the input-output pair, the Hamiltonian H is the total energy of the system, $\partial_{\mathbf{x}} = \frac{\partial}{\partial \mathbf{x}}$, J and M are skew-symmetric matrices, and matrices P, R and S satisfy

$$\begin{bmatrix} R & P \\ P^T & S \end{bmatrix} \geq 0 \tag{5}$$

As a consequence of the non-negative condition (5), H satisfies

$$H \leq H_0 + \int_0^t \mathbf{y}^T(\tau)\mathbf{u}(\tau)d\tau \tag{6}$$

where H_0 is the energy at $t = 0$. This result is equivalent to the numerical stability analysis presented in [2,3,13], i.e. the PHS formulation guarantees the model stability.

3. Mechanical model

In this section, we propose a port-Hamiltonian formulation of the wall motion. In an MSD system, there are two energy storage elements, namely, the mass that stores kinetic energy, and the spring that stores potential energy [23]. Thus, for a system with N_s interconnected MSD as shown in Figure 3, the total energy is given by

$$H_s = \frac{1}{2}\sum_{i=1}^{N_s}\left(\frac{\pi_i^2}{m_i} + k_i\bar{q}_i^2\right) + \frac{1}{2}\sum_{i=1}^{N_s-1} k_{ci}\left(\bar{q}_i - \bar{q}_{i+1}\right)^2 \tag{7}$$

where π_i is the momentum of mass m_i, k_i and k_{ci} are coefficients of lateral and coupling springs, and the relative mass displacements are given by $\bar{q}_i = q_i - q_{i0}$ where q_i is the mass position and q_{i0} is the equilibrium point when the flow velocity is equal to zero and the static pressure is equal to the reference pressure p_0.

Proposition 1. *Let H_s be the total energy of N_s interconnected MSD systems, as shown in Figure 3. Denoting by $\mathbf{q}_s = \begin{bmatrix}\bar{q}_1 & \bar{q}_2 & \cdots & \bar{q}_{N_s}\end{bmatrix}^T$ and $\pi_s = \begin{bmatrix}\pi_1 & \pi_2 & \cdots & \pi_{N_s}\end{bmatrix}^T$ the state variables associated with the displacement and momenta of masses, the finite-dimensional PHS approximation of the wall dynamics is given by*

$$\begin{bmatrix}\dot{\mathbf{q}}_s \\ \dot{\pi}_s\end{bmatrix} = \begin{bmatrix}\mathbf{0} & I \\ -I & -R_s\end{bmatrix}\begin{bmatrix}\partial_{\mathbf{q}_s} H_s \\ \partial_{\pi_s} H_s\end{bmatrix} + \begin{bmatrix}\mathbf{0} \\ I\end{bmatrix}\mathbf{u}_s \tag{8a}$$

$$\mathbf{y}_s = \begin{bmatrix}\mathbf{0} & I\end{bmatrix}\begin{bmatrix}\partial_{\mathbf{q}_s} H_s \\ \partial_{\pi_s} H_s\end{bmatrix} \tag{8b}$$

where the input $\mathbf{u}_s = \begin{bmatrix}F_1 & \cdots & F_{N_s}\end{bmatrix}^T$ is the set of external forces in each mass, the output $\mathbf{y}_s = \begin{bmatrix}v_{c1} & \cdots & v_{cN_s}\end{bmatrix}^T$ is the set of corresponding velocities, $\mathbf{0}$ and I are zero and identity matrices of proper dimensions, $\partial_{\mathbf{q}_s} H_s = K_s\mathbf{q}_s$ is the set of forces applied by the springs to the masses and $\partial_{\pi_s} H_s = \begin{bmatrix}\frac{\pi_1}{m_1} & \cdots & \frac{\pi_{N_s}}{m_{N-s}}\end{bmatrix}^T$ is the set of mass velocities. Matrices R_s and K_s are given by

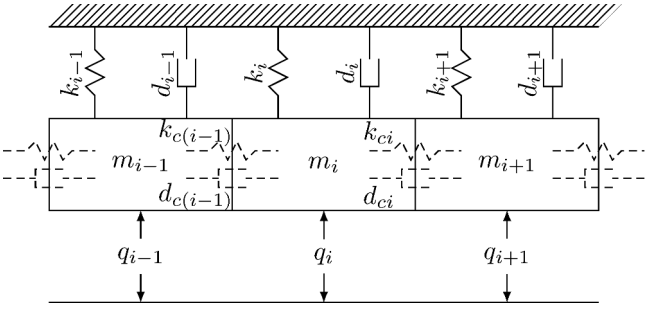

Figure 3. Mass-spring-damper (MSD) model for the different sections of the wall.

$$R_s = \begin{bmatrix} d_1 + d_{c1} & -d_{c1} & 0 & \cdots & \cdots & 0 \\ -d_{c1} & d_2 + d_{c1} + d_{c2} & -d_{c2} & \cdots & \cdots & 0 \\ 0 & -d_{c2} & d_3 + d_{c2} + d_{c3} & \ddots & \cdots & 0 \\ \vdots & \vdots & \ddots & \ddots & \ddots & \vdots \\ 0 & 0 & \cdots & \ddots & \ddots & -d_{c(N_s-1)} \\ 0 & 0 & \cdots & \cdots & -d_{c(N_s-1)} & d_{N_s} + d_{c(N_s-1)} \end{bmatrix} \tag{9}$$

$$K_s = \begin{bmatrix} k_1 + k_{c1} & -k_{c1} & 0 & \cdots & \cdots & 0 \\ -k_{c1} & k_2 + k_{c1} + k_{c2} & -k_{c2} & \cdots & \cdots & 0 \\ 0 & -k_{c2} & k_3 + k_{c2} + k_{c3} & \ddots & \cdots & 0 \\ \vdots & \vdots & \ddots & \ddots & \ddots & \vdots \\ 0 & 0 & \cdots & \ddots & \ddots & -k_{c(N_s-1)} \\ 0 & 0 & \cdots & \cdots & -d_{c(N_s-1)} & k_{N_s} + k_{c(N_s-1)} \end{bmatrix} \tag{10}$$

Proof. The velocity of one mass is the derivative of its displacement with respect to time, i.e. $\dot{\bar{q}}_i = \frac{\pi_i}{m_i} = \partial_{\pi_i} H_s$. Thus, for $\mathbf{q}_s$ we obtain

$$\dot{\mathbf{q}}_s = \partial_{\pi_s} H_s = \begin{bmatrix} \frac{\pi_1}{m_1} & \cdots & \frac{\pi_{N_s}}{m_{N_s}} \end{bmatrix}^T \tag{11}$$

On the other hand, applying a momentum balance on the masses, we obtain

$$\dot{\pi}_s = -\mathbf{F}_s - \mathbf{F}_d + \mathbf{u}_s \tag{12}$$

where $\mathbf{F}_s = [\, F_{s1} \quad \cdots \quad F_{sN_s} \,]^T$ is the set of forces applied by the springs to the masses, $\mathbf{F}_d = [\, F_{d1} \quad \cdots \quad F_{dN_s} \,]^T$ is the set of forces of the dampers, and $\mathbf{u}_s = [\, F_1 \quad \cdots \quad F_{N_s} \,]^T$ is the set of external forces. From Figure 3, we obtain that for the i-th mass, the spring force is given by

$$\begin{aligned} F_{si} &= k_i \bar{q}_i - k_{c(i-1)}(\bar{q}_{i-1} - \bar{q}_i) + k_{c(i)}(\bar{q}_i - \bar{q}_{i+1}) \\ &= \begin{bmatrix} -k_{c(i-1)} & k_i + k_{c(i)} + k_{c(i-1)} & -k_{c(i)} \end{bmatrix} \begin{bmatrix} \bar{q}_{i-1} \\ \bar{q}_i \\ \bar{q}_{i+1} \end{bmatrix} \\ &= \partial_{\bar{q}_i} H_s \end{aligned}$$

and the damper force is given by

$$\begin{aligned} F_{di} &= d_i v_{ci} + d_{ci}(v_{ci} - v_{c(i+1)}) + d_{c(i-1)}(v_{ci} - v_{c(i-1)}) \\ &= \begin{bmatrix} -d_{c(i-1)} & d_i + d_{c(i)} + d_{c(i-1)} & -d_{c(i)} \end{bmatrix} \begin{bmatrix} v_{c(i-1)} \\ v_{ci} \\ v_{c(i-1)} \end{bmatrix} \end{aligned}$$

where v_{ci} is the velocity of mass m_i. Considering $k_{c0} = k_{cN_s} = 0$ and $d_{c0} = d_{cN_s} = 0$ we obtain

$$\mathbf{F}_s = \partial_{\mathbf{q}_s} H_s = K_s \mathbf{q}_s \tag{13}$$

$$\mathbf{F}_d = R_s \partial_{\pi_s} H_s \tag{14}$$

where R_s and K_s are given by (9) and (10), respectively. Thus, using (13) and (14), the momentum balance in (12) can be rewritten as

$$\dot{\pi}_s = -\partial_{\mathbf{q}_s} H_s - R_s \partial_{\pi_s} H_s + \mathbf{u}_s \tag{15}$$

Finally, defining the state vector as $\mathbf{x}^T = \begin{bmatrix} \mathbf{q}_s^T & \pi_s^T \end{bmatrix}$, the ODEs (11) and (15) can be rewritten in the PHS form (4), where

$$J = \begin{bmatrix} \mathbf{0} & I \\ -I & \mathbf{0} \end{bmatrix} R = \begin{bmatrix} \mathbf{0} & \mathbf{0} \\ \mathbf{0} & R_s \end{bmatrix} g = \begin{bmatrix} \mathbf{0} \\ I \end{bmatrix},$$

and where the matrices P, M and S are equal to zero, obtaining the model described in (8).□

4. Fluid model

In this section, we propose a port-Hamiltonian model for incompressible fluids in tubes with time-varying geometries. As mentioned before, we consider flows with Match number $M < 0.3$ and provide a 1D model of the fluid using incompressible sections and infinitesimal compressible zones called nodes. From an energy point of view, incompressible sections are kinetic energy storage elements, describing the fluid motion through the momentum balance:

$$\rho_0 \partial_t \mathbf{v} = -\rho_0 \mathbf{v} \cdot \quad \mathbf{v} - \quad p - \mu \quad ^2\mathbf{v} \tag{16}$$

subject to $\quad \cdot (\mathbf{v}) = 0$, where ρ_0 is the reference density of the fluid and $\mathbf{v} = [v \mathrm{v}]^T$ with v and v as the longitudinal and transverse velocities of the fluid, respectively. Similarly, nodes store potential energy and are used to describe the pressure distribution in the flow. Their dynamics are governed by the changes of the fluid density. Then, the fluid dynamics in a node is given by

$$\partial_t \rho = - \quad \cdot (\rho \mathbf{v}) \tag{17}$$

On the other hand, the loss of kinetic energy of a fluid in a tube is given by different phenomena [25], such as viscosity friction with the walls, turbulences and irregularities in the geometry. Thus, we firstly discuss the energy dissipation in the flow, and then we present the models for the incompressible sections and for the nodes to develop a scalable model.

4.1. Power dissipation in the flow

Note that the term $\mu \quad ^2\mathbf{v}$ in (2) is the incompressible simplification of $- \quad \cdot (\tau)$, where τ is the viscous stress tensor for Newtonian fluids [25]. The dissipation in the flow can be

obtained from the dot product $-(\mathbf{v}\cdot\quad\cdot(\tau)) = -(\quad\cdot(\tau\cdot\mathbf{v})) - (-\tau:\quad\mathbf{v})$, where the term $(-\tau:\quad\mathbf{v})$ is the scalar product between the tensors τ and $\quad\mathbf{v}$, and it is always positive, describing the power dissipation in the flow [25]. For incompressible flows, the viscous dissipation has the general form:

$$D_v = \int(-\tau:\quad\mathbf{v})dV = \lambda\frac{1}{2}\rho A_v v_v^3 \geq 0 \tag{18}$$

where v_v and A_v are the characteristic velocity and area, respectively, and $\lambda = \lambda_\mu + \lambda_g$, where λ_μ is the friction loss factor that depends on the Reynolds number and λ_g is the loss factor associated with the tube geometry. Note that, from Assumption 2, the transversal flow velocity has an algebraic relation with v_{ci}. As a consequence, the dissipation is given by the longitudinal flow component. Thus, in the i-th section of the flow with density ρ_0, the viscous dissipation can be written as

$$D_{vi} = \lambda_i\frac{1}{2}\rho_0 A_i v_i^2|v_i| \tag{19}$$

The loss factor λ_μ can be chosen depending on the considered assumptions on the flow, see, e.g. [25, Section 6.2]. On the other hand, λ_g depends on the geometry of the tube and, in the literature, there exist empirical formulas for tube expansions and contractions, change of direction and different classes of bifurcation junctions [28,29]. In this work, we only consider the loss factors associated with sudden expansions and contractions. In a sudden expansion, when the fluid enters a section with an enlarged cross-sectional area, a jet is formed as the fluid separates from the wall of the smaller tube section. This jet flow expands until it fills the entire area and part of the fluid breaks away and circulates in the corner of the expanded section [28]. In this case, the loss factor is given by

$$\lambda_i^e = \left(1 - \frac{A_i}{A_{i+1}}\right)^2 \tag{20}$$

where A_i is the cross-sectional area of the i-th incompressible section.

In a sudden contraction, given the reduction of the tube, the fluid accelerates as it enters the smaller section. In this case, the loss factor is given by [28]

$$\lambda_i^c = \frac{1}{2}\left(1 - \frac{A_i}{A_{i-1}}\right) \tag{21}$$

According to [30], the loss factor in the inlet depends on the entrance tube geometry and is usually less than 0.78, while the loss factor associated with the outlet is equal to 1.

4.2. Model of incompressible fluid sections

If we consider the i-th section of the fluid, the upper boundary moves in the transverse direction with velocity v_{ci}, as shown in Figure 4. Moreover, as a consequence of Assumption 1, a change of density in a node implies a change of the corresponding volume, which generates a variation in the volume of adjacent incompressible sections. The first effect of these moving boundaries is that the volume of the i-th incompressible section is a function of the density of adjacent nodes. Thus, considering a node length of

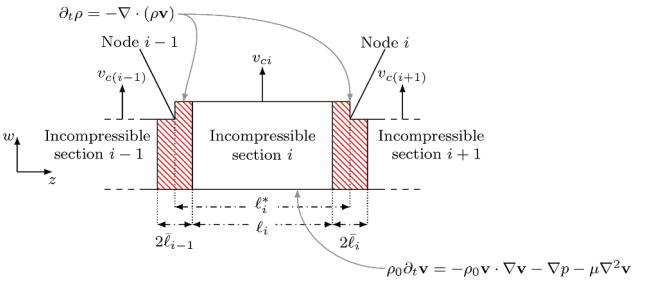

Figure 4. Coupling incompressible fluid sections using nodes with compressible behaviour.

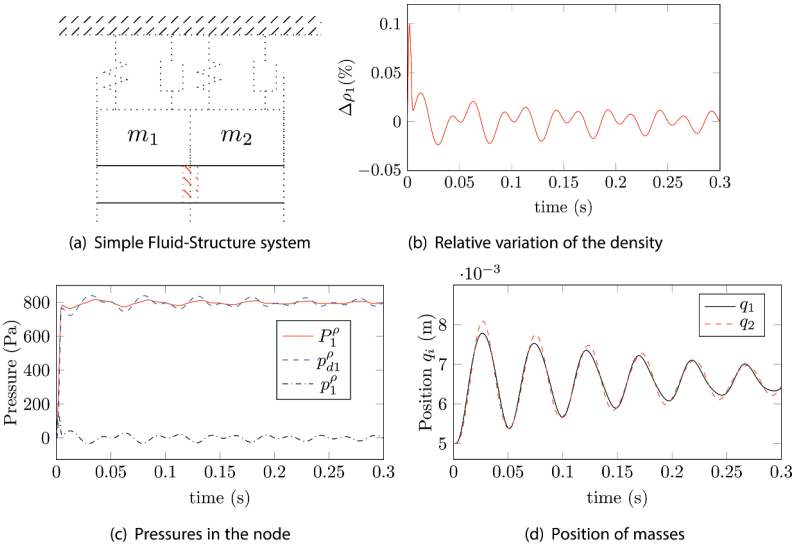

Figure 5. (a) Simple Fluid-Structure Interaction system for numerical example of Section 6.1. (b) Relative variation of density ρ_1 in the node. (b) Behaviour of pressures in the node, p_1^ρ: static pressure, p_{d1}^ρ: dynamic pressure, P_1^ρ: total pressure. (d) Position of masses, $q_1 = \bar{q}_1 + q_{10}$: position of mass m_1, $q_2 = \bar{q}_2 + q_{20}$: position of mass m_2

$2\bar{\ell}_i$, as shown in Figure 4, the node volume is given by $\bar{V}_i = \bar{\ell}_i(A_i + A_{i+1})$, where A_i and A_{i+1} are the cross-sectional areas of the adjacent incompressible flow sections. Thus, the volume V_i of section i is described by a fixed reference value $V_i^* = A_i \ell_i^*$ minus the corresponding part of adjacent nodes, see Figure 4, i.e.

$$V_i = V_i^* - A_i(\bar{\ell}_i + \bar{\ell}_{i-1}) = V_i^* - \frac{\kappa}{\rho_i}\alpha_i - \frac{\kappa}{\rho_{i-1}}(1 - \alpha_{i-1}) \tag{22}$$

where $\alpha_i = A_i/(A_i + A_{i+1})$ is a dimensionless factor. As we will see in the next subsection, the description of V_i in (22) will help us to describe the dynamic pressure in each node.

The second effect of these moving boundaries is that part of the fluid moves in the transverse direction, induced by the boundary velocity v_{ci}. This implies that the

longitudinal flow in the section is affected by the upper wall movement. As a consequence, from (1), we obtain the following relationship:

$$Q_{1i} - Q_{2i} - A_{ci}v_{ci} = 0 \tag{23}$$

where A_{ci} is the contact area of the fluid section with the moving boundary. Note that the inlet and outlet flows in a section Q_{1i} and Q_{2i} respectively, are different when the upper wall moves. Thus, denoting by v_i the average longitudinal flow velocity in section i, to satisfy (23), we define the inlet and outlet flows as

$$Q_{1i} = A_i v_i + \frac{1}{2}A_{ci}v_{ci} \tag{24}$$

$$Q_{2i} = A_i v_i - \frac{1}{2}A_{ci}v_{ci} \tag{25}$$

where $A_i v_i$ is the average longitudinal flow and $A_{ci}v_{ci}$ is the transverse flow in the contact surface of the moving boundary. Note that (24) and (25) are equal when the upper boundary does not move.

The third effect of the moving boundaries is that the tube geometry is time varying, inducing a fluid rotation in each section. To simplify the model, we consider a two-dimensional flow and the following assumption

Assumption 2. *Denote by* v *the transverse component of the flow velocity. The gradient of* v *is uniform in each fluid section and is given by* $\partial_w \mathrm{v} = v_{ci}/q_i$ *and* $\partial_z \mathrm{v} = 0$ *where w and z denote the transversal and longitudinal axis respectively, and* q_i *is the moving boundary position.*

Note that, from Assumption 2, the transversal velocity in a section i is given by $\mathrm{v} = v_{ci}w/q_i$. As a consequence, the corresponding transversal momentum satisfies the following algebraic relationship with the boundary velocity $\pi_{yi} = \int \rho_0 \mathrm{v} dV_i = \rho_0 V_i v_{ci}/2$. This algebraic constraint implies that the dynamics of the transversal momentum in each incompressible section are given by a linear combination of the ODEs associated with the mechanical model, which were shown above, and the ODEs that describe density behaviour in the nodes.

Thus, to obtain a minimal realization we consider the following proposition to describe the flow in one incompressible section.

Proposition 2. *In a fluid section with volume* V_i *and uniform gradient of transversal velocity, the flow is described by the longitudinal flow momentum dynamics*:

$$\dot{\pi}_{zi} = -A_i \frac{\lambda_i}{2}\rho_0 |v_i| v_i - A_{ci}\rho_0 v_i v_{ci} + A_i(P_{1i} - P_{2i}) \tag{26}$$

where the term $A_{ci}\rho_0 v_i v_{ci}$ *represents the effect of the moving boundary in the longitudinal flow.*

Proof. As we mentioned above, the corresponding transversal momentum has an algebraic relationship with the boundary velocity, i.e. the boundary velocity defines the

transversal behaviour of the flow. Thus, it is only necessary to know the longitudinal flow momentum to describe the fluid in one section. Then, from (16) we obtain that

$$\rho_0 \partial_t v + \rho_0 v \partial_z v + \rho_0 \mathrm{v} \partial_w v + \partial_z p = \mu\left(\partial_z^2 v + \partial_w^2 v\right) \tag{27}$$

where the term $\rho \mathrm{v} \partial_w v$ is associated with the conversion of longitudinal flow into transversal flow and vice versa, induced by the velocity of the boundary. Integrating in the section volume the first and third terms of (29) and applying the Leibniz integral rule and the divergence theorem, an additional term associated with the contact surface S_{ci} and its correspondence velocity v_{ci} appears, i.e.

$$\begin{aligned}\int \rho_0 \partial_t v + \rho_0 \mathrm{v} \partial_w v dV_i &= \dot{\pi}_{zi} + A_i \frac{\rho_0}{2}\left(\left(\frac{Q_{2i}}{A_i}\right)^2 - \left(\frac{Q_{1i}}{A_i}\right)^2\right) \\ &= \dot{\pi}_{zi} + A_{ci}\rho_0 v_i v_{ci}\end{aligned} \tag{28}$$

Integrating the remaining terms of (27) and considering a uniform velocity in the inlet and outlet cross-sectional surfaces of V_i we obtain

$$\int \partial_z\left(\frac{\rho_0}{2} v^2 + p\right) dV_i = -A_i(P_{1i} - P_{2i}) \tag{29}$$

where P_{1i} and P_{2i} are the inlet and outlet total pressures, respectively. Finally, in this work we only consider the power dissipation of the stress tensor. Then, the term $\int \mu\left(\partial_z^2 v + \partial_w^2 v\right) dV_i$ represents the force associated with the viscous dissipation. Thus, using (19) this force can be approximated as

$$\int \mu\left(\partial_z^2 v + \partial_w^2 v\right) dV_i \approx -A_i \lambda_i \frac{1}{2} \rho_0 |v_i| v_i \tag{30}$$

Finally, combining (28), (29) and (30), and solving for $\dot{\pi}_{zi}$ we obtain (26).

If we now consider the kinetic energy in one section, we can express it as $K_i = \frac{1}{2}\rho_0 V_i v_i^2 = \frac{1}{2}\pi_{zi}^2/(\rho_0 V_i)$. Thus, for N sections the total kinetic energy is

$$K_f = \sum_{i=1}^{N} \frac{1}{2} \frac{\pi_{zi}^2}{\rho_0 V_i} \tag{31}$$

where $\partial_{\pi_{zi}} K_f = \pi_{zi}/(\rho_0 V_i) = v_i$ is the average velocity in section i. Using the PHS framework we describe the flow dynamics in N section as shown in Proposition 3.

Proposition 3. *Consider a fluid domain divided into N incompressible sections and $N-1$ nodes. Defining the state vector $\mathbf{p}_z$ as the set of longitudinal momenta of incompressible sections, $\mathbf{P}_1$ and $\mathbf{P}_2$ as the total pressure sets at the inlet and outlet boundaries of the sections, respectively, $\mathbf{u}_b$ as the set of upper boundary velocities, $\mathbf{Q}_1$ and $\mathbf{Q}_2$ as the inlet and outlet flow sets, respectively, and $\mathbf{F}_\pi^* = \mathbf{F} + \hat{\mathbf{F}}$ where $\mathbf{F}$ is the set of forces applied over the contact area of sections with the moving wall and $\hat{F}$ is an additional term. Then, the port-Hamiltonian model that describes the dynamics of incompressible sections is given by*

$$\dot{\pi}_z = -R_f \partial_{\pi_z} K_f + \begin{bmatrix} \vartheta_\pi^T \\ -\vartheta_\pi^T \\ -\varphi_\pi^T \end{bmatrix}^T \begin{bmatrix} \mathbf{P}_1 \\ \mathbf{P}_2 \\ \mathbf{u}_b \end{bmatrix} \tag{32a}$$

$$\begin{bmatrix} \mathbf{Q}_1 \\ -\mathbf{Q}_2 \\ -\mathbf{F}_\pi^* \end{bmatrix} = \begin{bmatrix} \vartheta_\pi^T \\ -\vartheta_\pi^T \\ -\varphi_\pi^T \end{bmatrix} \partial_{\mathbf{p}_z} K_f + \begin{bmatrix} \mathbf{0} & \mathbf{0} & \psi_\pi \\ \mathbf{0} & \mathbf{0} & \psi_\pi \\ -\psi_\pi^T & -\psi_\pi^T & \mathbf{0} \end{bmatrix} \begin{bmatrix} \mathbf{P}_1 \\ \mathbf{P}_2 \\ \mathbf{u}_b \end{bmatrix} \tag{32b}$$

where $R_f = diag([\, r_1 \quad \cdots \quad r_N \,])$ *is the dissipation matrix of the flow,* $\vartheta_\pi = diag([\, A_1 \quad \cdots \quad A_N \,])$ *maps the boundary pressures of the sections,* $\varphi_\pi = diag([\, A_{c1}\pi_{z1}/V_1 \quad \cdots \quad A_{cN}\pi_{zN}/V_N \,])$ *and* $\psi_\pi = diag([\, A_{c1}/2 \quad \cdots \quad A_{cN}/2 \,])$.

Proof. Let $v_i = \partial_{\pi_{zi}} K_f = \pi_{zi}/(\rho_0 V_i)$ and $r_i = \lambda_i \rho_0 |\pi_{zi}|/(2\ell_i)$. Then, rewriting (26), the longitudinal flow momentum equation in a section i is given by

$$\dot{\pi}_{zi} = -r_i \partial_{\pi_{zi}} K_f - \frac{A_{ci}\pi_{zi}}{V_i} v_{ci} + A_i (P_{1i} - P_{2i}) \tag{33}$$

where the inlet and outlet pressures P_{1i} and P_{2i} and the velocity v_{ci} are inputs. The power conjugated outputs associated with these inputs are the inlet and outlet flows Q_{1i} and Q_{2i} and the force $F_{\pi i}$ applied to the contact surface. From (24) and (25) we obtain

$$Q_{1i} = A_i \partial_{\pi_{zi}} K_f + \frac{A_{ci}}{2} v_{ci} \tag{34}$$

$$Q_{2i} = A_i \partial_{\pi_{zi}} K_f - \frac{A_{ci}}{2} v_{ci} \tag{35}$$

Define an auxiliary force F_i^* as

$$F_{\pi i}^* = A_{ci} \left(\frac{\pi_{zi}}{V_i} \partial_{\pi_{zi}} K_f + (P_{1i} + P_{2i})/2 \right) \tag{36}$$

$$= F_{\pi i} + \hat{F}_{\pi i} \tag{37}$$

where $\hat{F}_{\pi i}$ is an extra term that is compensated in the interconnection with the mechanical model, as shown in Section 5. Thus, the PHS model that describes the dynamics of the i-th section is given by

$$\dot{\pi}_{zi} = -r_i \partial_{\pi_{zi}} K_f + \begin{bmatrix} A_i & -A_i & -\frac{A_{ci}\pi_{zi}}{V_i} \end{bmatrix} \begin{bmatrix} P_{1i} \\ P_{2i} \\ v_{ci} \end{bmatrix}$$

$$\begin{bmatrix} Q_{1i} \\ -Q_{2i} \\ -F_i^* \end{bmatrix} = \begin{bmatrix} A_i \\ -A_i \\ -\frac{A_{ci}\pi_{zi}}{V_i} \end{bmatrix} \partial_{\pi_{zi}} K_f + \begin{bmatrix} \mathbf{0} & M_i \\ -M_i^T & 0 \end{bmatrix} \begin{bmatrix} P_{1i} \\ P_{2i} \\ v_{ci} \end{bmatrix}$$

where $M_i = [\, A_{ci}/2 \quad A_{ci}/2 \,]^T$.

Finally, for N incompressible sections, we define the state vector as $\mathbf{p}_z = [\,\pi_{z1} \cdots \pi_{zN}\,]^T$. Denoting by $\mathbf{P}_1 = [\,P_{11} \cdots P_{1N}\,]^T$ and $\mathbf{P}_2 = [\,P_{21} \cdots P_{2N}\,]^T$ the inlet and outlet total pressure sets, respectively, $\mathbf{u}_b = [\,v_{c1} \cdots v_{cN}\,]^T$ the set of section velocities in contact surfaces; $\mathbf{Q}_1 = [\,Q_{11} \cdots Q_{1N}\,]^T$, and $\mathbf{Q}_2 = [\,Q_{21} \cdots Q_{2N}\,]^T$ the inlet and outlet flow sets, and $\mathbf{F}_\pi^* = \mathbf{F}_\pi + \hat{\mathbf{F}}_\pi$ where $\mathbf{F}_\pi = [\,F_{\pi 1} \cdots F_{\pi N}\,]^T$ and $\hat{\mathbf{F}}_\pi = \left[\,\hat{F}_{\pi 1} \cdots \hat{F}_{\pi N}\,\right]^T$, and defining matrices $R_f = diag([\,r_1 \cdots r_N\,])$, $\vartheta_\pi = diag([\,A_1 \cdots A_N\,])$, $\varphi_\pi = diag([\,A_{c1}\pi_{z1}/V_1 \cdots A_{cN}\pi_{zN}/V_N\,])$, $\psi_\pi = diag([\,A_{c1}/2 \cdots A_{cN}/2\,])$, then, we obtain the PHS shown in (32).□

4.3. Model of nodes

As explained in Assumption 1, the density in each node is assumed to be uniform. Then, the continuity equation in (17) can be rewritten as

$$\partial_t \rho + \rho \quad \cdot (\mathbf{v}) = 0 \tag{38}$$

This density variation implies a change in the node pressure, which, in turn, has an associated energy. We denote by $p_j^\rho = p_j - p_0$ the pressure variation in the j-th node, where p_0 is the pressure at the reference density ρ_0 and p_j is the absolute pressure in the node. Thus, from the definition of the bulk modulus, β_S [31], we obtain

$$p_j^\rho = \beta_S \ln\left(\frac{\rho_j}{\rho_0}\right) \tag{39}$$

Considering that the mass in each node is small, the kinetic energy can be neglected. From the first law of thermodynamics and considering an adiabatic process, the potential energy E_j, is given by the fluid work, $dE_j = -p_j^\rho\, dV_j$. Using (3), the differential of the potential energy can be written as

$$dE_j = p_j^\rho \frac{\kappa}{\rho_j^2} d\rho_j \tag{40}$$

where p_j^ρ is the node pressure.

The potential energy in node j is then given by the following non-negative function

$$E_j = \kappa\beta_S \frac{\rho_j - \rho_0\Big(1 + \ln(\rho_j/\rho_0)\Big)}{\rho_j \rho_0} \tag{41}$$

Thus, for $N-1$ nodes, the total energy is

$$E_f = \sum_{j=1}^{N-1} \kappa\beta_S \frac{\rho_j - \rho_0\Big(1 + \ln(\rho_j/\rho_0)\Big)}{\rho_j \rho_0} \tag{42}$$

The PHS that describes the density dynamics is then given in the following proposition.

Proposition 4. *Consider a fluid domain divided into N incompressible sections and N − 1 nodes. Denoting by* $\mathbf{r}$ *the set of node densities, by* $\mathbf{Q}_1^\rho$ *and* $\mathbf{Q}_2^\rho$ *the inlet and outlet boundary*

flow sets of nodes, $\mathbf{p}_1^\rho$ *and* $\mathbf{p}_2^\rho$ *the inlet and outlet static pressure sets at the inlet and outlet node boundaries, respectively, and* F_ρ *as the set of forces applied by nodes in adjacent wall sections. Then, the density dynamics are given by the following PHS*:

$$\dot{\rho} = \mathbf{0}\partial_\rho E_f + \begin{bmatrix} \vartheta_\rho^T \\ -\vartheta_\rho^T \\ -\varphi_\rho^T \end{bmatrix}^T \begin{bmatrix} \mathbf{Q}_1^\rho \\ \mathbf{Q}_2^\rho \\ \mathbf{u}_b \end{bmatrix} \tag{43a}$$

$$\begin{bmatrix} \mathbf{p}_1^\rho \\ -\mathbf{p}_2^\rho \\ -\mathbf{F}_\rho \end{bmatrix} = \begin{bmatrix} \vartheta_\rho^T \\ -\vartheta_\rho^T \\ -\varphi_\rho^T \end{bmatrix} \partial_\rho E_f \tag{43b}$$

where $\vartheta_\rho = diag\left(\left[\rho_1^2/\kappa \cdots \rho_{N-1}^2/\kappa\right]\right)$ *is the matrix mapping the inlet and outlet flows in nodes. The matrix* $\varphi_\rho = \vartheta_\rho([g_{An} \quad 0_{N-1\times 1}] + [0_{N-1\times 1} \quad g_{An}])$ *with* $g_{An} = diag\left(\left[A_{n1} \quad \cdots \quad A_{n(N-1)}\right]\right)$, *maps the upper boundary velocities in nodes.*

Proof. Integrating (38) over the j-th node volume, we obtain that the node density is affected by the adjacent moving boundaries, i.e.

$$\dot{\rho}_j = \frac{\rho_j^2}{\kappa}\left(Q_{1j}^\rho - Q_{2j}^\rho\right) - A_{nj}\frac{\rho_j^2}{\kappa}\left(v_{cj} + v_{c(j+1)}\right) \tag{44}$$

where Q_{1j}^ρ and Q_{2j}^ρ are the inlet and outlet flows of the node, respectively, v_{cj} and $v_{c(j+1)}$ are the velocities of adjacent moving boundaries, and A_{nj} is the corresponding contact area. The power conjugate variables for the inlet and outlet flows are the internal node pressures. Then, from Assumption 1 and (40), we obtain

$$p_{1j} = p_{2j} = \frac{\rho_j^2}{\kappa}\partial_{\rho_j} E_f \tag{45}$$

Similarly, the conjugated variables associated with the velocity of adjacent moving boundaries are the applied forces. Then, as shown in Figure 4, in the j-th wall section the force applied on the contact surface for the nodes is given by

$$F_{j\rho} = A_{n(j-1)}\frac{\rho_{j-1}^2}{\kappa}\partial_{\rho_{j-1}} E_f + A_{nj}\frac{\rho_j^2}{\kappa}\partial_{\rho_j} E_f \tag{46}$$

Thus, for $N-1$ nodes, the density dynamics can be described using the PHS model in 2, where the matrices J, R, P, M and S are equal to zero, the input is given by $\mathbf{u} = [(\mathbf{Q}_1^\rho)^T(\mathbf{Q}_2^\rho)^T\mathbf{u}_b^T]^T$ with $\mathbf{Q}_1^\rho = [Q_{11}^\rho \cdots Q_{1N}^\rho]^T$ and $\mathbf{Q}_2^\rho = [Q_{21}^\rho \cdots Q_{2N}^\rho]^T$, the output is given by $\mathbf{y} = [(\mathbf{p}_1^\rho)^T - (\mathbf{p}_2^\rho)^T - \mathbf{F}_\rho^T]^T$ with $\mathbf{p}_1^\rho = [p_{11}^\rho \cdots p_{1N}^\rho]^T$, $\mathbf{p}_2^\rho = [p_{21}^\rho \cdots p_{2N}^\rho]^T$ and $\mathbf{F}_\rho = [F_{1\rho} \cdots F_{N\rho}]^T$, and the matrix $g = [\vartheta_\rho \ -\vartheta_\rho \ -\varphi_\rho]$ where $\vartheta_\rho = diag\left(\left[\rho_1^2/\kappa \cdots \rho_{N-1}^2/\kappa\right]\right)$ is the matrix mapping the inlet and outlet flows in nodes, $\varphi_\rho = \vartheta_\rho([g_{An} \quad 0_{N-1\times 1}] + [0_{N-1\times 1} \quad g_{An}])$ is the matrix mapping the upper boundary velocities in nodes, with $g_{An} = diag\left(\left[A_{n1} \cdots A_{n(N-1)}\right]\right)$. Then we obtain the PHS formulation in (43).□

4.4. Scalable flow model

In this section, we develop the interconnection between N sections and $N-1$ nodes to obtain the flow model. The set of differential equations for incompressible sections and nodes is given by (32) and (43), respectively. Note that when two PHS are coupled via a power-preserving interconnection, the model obtained is port-Hamiltonian and the total energy is the sum of the energies of each subsystem [22,23]. Then, in our model, the total energy of the flow is given by

$$H_f = K_f + E_f \tag{47}$$

Note that the outputs $\mathbf{Q}_1$ and $\mathbf{Q}_2$ of the incompressible section model are compatible with the inputs $\mathbf{Q}_1^\rho$ and $\mathbf{Q}_2^\rho$ of the node model. Similarly, the inputs $\mathbf{P}_1$ and $\mathbf{P}_2$ are compatible with outputs $\mathbf{p}_1^\rho$ and $\mathbf{p}_2^\rho$. However, note that $\mathbf{p}_1^\rho$ and $\mathbf{p}_2^\rho$ are static pressure and $\mathbf{P}_1$ and $\mathbf{P}_2$ are total pressures. Thus, we describe the flow dynamics as shown in the following proposition.

Proposition 5. *Let $\mathbf{P}_1^\rho = \mathbf{p}_1^\rho + \mathbf{p}_d^\rho$ and $\mathbf{P}_2^\rho = \mathbf{p}_2^\rho + \mathbf{p}_d^\rho$ be the total pressure sets at the inlet and outlet boundaries of nodes where $\mathbf{p}_d^\rho$ is the set of dynamic pressures in the nodes, $\{P_i, Q_i\}$ and $\{P_o, Q_o\}$ the pairs of total pressure and flow at the inlet and outlet boundaries of the fluid domain, respectively. Then, there exist matrices C_1, C_2, C_{1*} and C_{2*}, such that*

$$\begin{bmatrix} C_1 \\ C_{1*} \end{bmatrix} : \mathbf{Q}_1 \to \begin{bmatrix} \mathbf{Q}_2^\rho \\ Q_i \end{bmatrix}, \begin{bmatrix} C_2 \\ C_{2*} \end{bmatrix} : \mathbf{Q}_2 \to \begin{bmatrix} \mathbf{Q}_1^\rho \\ Q_o \end{bmatrix}, \begin{bmatrix} C_1 \\ C_{1*} \end{bmatrix}^T : \begin{bmatrix} \mathbf{p}_2^\rho + \mathbf{p}_d^\rho \\ P_i \end{bmatrix} \to \mathbf{P}_1, \text{and} \begin{bmatrix} C_2 \\ C_{2*} \end{bmatrix}^T : \begin{bmatrix} \mathbf{p}_1^\rho + \mathbf{p}_d^\rho \\ P_o \end{bmatrix} \to \mathbf{P}_2.$$

Thus, the scalable port-Hamiltonian formulation for a flow with moving boundary is given by:

$$\begin{bmatrix} \dot{\pi}_z \\ \dot{\rho} \end{bmatrix} = \begin{bmatrix} -R_f & \boldsymbol{\phi} \\ -\boldsymbol{\phi}^T & \mathbf{0} \end{bmatrix} \begin{bmatrix} \partial_{\pi_z} H_f \\ \partial_\rho H_f \end{bmatrix} + \begin{bmatrix} \vartheta & -\varphi_\pi \\ \mathbf{0} & -\varphi \end{bmatrix} \begin{bmatrix} \mathbf{u}_p \\ \mathbf{u}_b \end{bmatrix} \tag{48a}$$

$$\begin{bmatrix} \mathbf{y}_Q \\ \mathbf{y}_b \end{bmatrix} = \begin{bmatrix} \vartheta^T & \mathbf{0} \\ -\varphi_\pi^T & -\varphi^T \end{bmatrix} \begin{bmatrix} \partial_{\pi_z} H_f \\ \partial_\rho H_f \end{bmatrix} + \begin{bmatrix} \mathbf{0} & \psi \\ -\psi^T & \mathbf{0} \end{bmatrix} \begin{bmatrix} \mathbf{u}_p \\ \mathbf{u}_b \end{bmatrix} \tag{48b}$$

where $\mathbf{u}_p = [P_i\, P_o]^T$, $\mathbf{y}_Q = [Q_i\ -Q_o]^T$ and y_b contains the forces applied by the flow to the contact surfaces of the moving wall. Matrix $\vartheta = \vartheta_\pi \begin{bmatrix} C_{1*}^T & -C_{2*}^T \end{bmatrix}$ maps the boundary pressures in the corresponding fluid sections, matrix $\varphi = \varphi_\rho + \vartheta_\rho (C_2 + C_1)\psi_\pi$ maps the upper boundary velocities in the nodes, and $\boldsymbol{\phi} = \vartheta_\pi (C_1^T - C_2^T)\vartheta_\rho^T$, $\psi = \begin{bmatrix} C_{1*}^T & C_{2*}^T \end{bmatrix}^T \psi_\pi$.

Proof. Note that $Q_i = Q_{11}$ and $Q_{2(i-1)}^\rho = Q_{1i}$, $i \in [2, N]$. Similarly, $Q_o = Q_{2N}$ and $Q_{1i}^\rho = Q_{2i}$, $i \in [1, N-1]$. Then, defining the matrices C_1, C_2, C_{1*} and C_{2*} as

$$\begin{bmatrix} C_{1*} \\ C_1 \end{bmatrix} = \begin{bmatrix} 1 & 0_{1\times N-1} \\ 0_{N-1\times 1} & I \end{bmatrix} \qquad \begin{bmatrix} C_2 \\ C_{2*} \end{bmatrix} = \begin{bmatrix} I & 0_{N-1\times 1} \\ 0_{1\times N-1} & 1 \end{bmatrix} \tag{49}$$

we obtain the power conserving interconnection rule given by

$$\begin{bmatrix} \mathbf{Q}_1^\rho \\ \mathbf{Q}_2^\rho \\ \mathbf{P}_1 \\ \mathbf{P}_2 \\ -Q_i \\ Q_o \end{bmatrix} = [cccc|cc\mathbf{000} - C_2\mathbf{00} \tag{59}$$

$$\mathbf{00}C_1\mathbf{000} \tag{60}$$

$$\mathbf{0} - C_1^T\mathbf{00}C_{1*}^T\mathbf{0} \tag{61}$$

$$C_2^T\mathbf{0000}C_{2*}^T \tag{62}$$

$$\mathbf{00} - C_{1*}\mathbf{000} \tag{63}$$

$$\mathbf{000} - C_{2*}\mathbf{00}] \begin{bmatrix} \mathbf{p}_1^\rho + \mathbf{p}_d^\rho \\ -\mathbf{p}_2^\rho - \mathbf{p}_d^\rho \\ \mathbf{Q}_1 \\ -\mathbf{Q}_2 \\ P_i \\ P_o \end{bmatrix} \tag{64}$$

Thus, the models (32) and (43) can be rewritten as

$$\underline{\mathbf{p}}_z = -R_f\partial_{\mathbf{p}_z}K_f + \vartheta_\pi C_1^T\left(\mathbf{p}_2^\rho + \mathbf{p}_d^\rho\right) - \vartheta_\pi C_2^T\left(\mathbf{p}_1^\rho + \mathbf{p}_d^\rho\right) + \vartheta_\pi C_{1*}^T P_i - \vartheta_\pi C_{2*}^T P_o \tag{65}$$

$$\underline{\mathbf{r}} = -\varphi_\rho\mathbf{u}_b + \vartheta_\rho C_2\left(\vartheta_\pi^T\partial_{\mathbf{p}_z}K_f - \psi_\pi\mathbf{u}_b\right) - \vartheta_\rho C_1\left(\vartheta_\pi^T\partial_{\mathbf{p}_z}K_f + \psi_\pi\mathbf{u}_b\right) \tag{66}$$

Considering $\partial_{\mathbf{p}_z}K_f = \partial_{\mathbf{p}_z}H_f$ and from Proposition 4, we have that $\mathbf{p}_1^\rho = \mathbf{p}_2^\rho = \vartheta_\rho^T\partial_{\mathbf{r}}E_f$. To define p_d^ρ it is necessary to obtain a description of the dynamic pressure in each node. From (24) we obtain

$$\partial_{\rho_i}K_f = \frac{\rho_0}{2}\left(\frac{\pi_{zi}}{\rho_0 V_i}\right)^2\partial_{\rho_i}V_i + \frac{\rho_0}{2}\left(\frac{\pi_{z(i+1)}}{\rho_0 V_{i+1}}\right)^2\partial_{\rho_i}V_{i+1} = \frac{\kappa}{\rho_i^2}p_{di}^\rho \tag{67}$$

where $p_{di}^\rho = \frac{\rho_0}{2}\left(\frac{\pi_{zi}}{\rho_0 V_i}\right)^2\alpha_i + \frac{\rho_0}{2}\left(\frac{\pi_{z(i+1)}}{\rho_0 V_{i+1}}\right)^2(1-\alpha_i)$ is the dynamic pressure in the i-th node. Then, for $N-1$ nodes, the set of dynamic pressures is given by $\mathbf{p}_d^\rho = \vartheta_\rho^T\partial_\rho K_f$. This implies that $\mathbf{p}_1^\rho + \mathbf{p}_d^\rho = \mathbf{p}_2^\rho + \mathbf{p}_d^\rho$ where $\mathbf{p}_1^\rho + \mathbf{p}_d^\rho = \vartheta_\rho^T\partial_{\mathbf{r}}K_f + \vartheta_\rho^T\partial_{\mathbf{r}}E_f = \vartheta_\rho^T\partial_{\mathbf{r}}H_f$, i.e. the flow dynamics can be rewritten as

$$\underline{\mathbf{p}}_z = -R_f\partial_{\mathbf{p}_z}H_f + \vartheta_\pi\left(C_1^T - C_2^T\right)\vartheta_\rho^T\partial_{\mathbf{r}}H_f + \vartheta_\pi C_{1*}^T P_i - \vartheta_\pi C_{2*}^T P_o \tag{68}$$

$$\underline{\mathbf{r}} = \vartheta_\rho(C_2 - C_1)\vartheta_\pi^T\partial_{\mathbf{p}_z}H_f - \left(\varphi_\rho + \vartheta_\rho(C_2 - C_1)\psi_\pi\right)\mathbf{u}_b \tag{69}$$

Finally, defining $\boldsymbol{\phi} = \vartheta_\pi \left(C_1^T - C_2^T\right)\vartheta_\rho^T$, $\vartheta = \vartheta_\pi [C_{1*}^T - C_{2*}^T]$, $\varphi = \varphi_\rho + \vartheta_\rho (C_2 - C_1)\psi_\pi$ and $\psi = [C_{1*}^T\, C_{2*}^T]^T \psi_\pi$, the previous dynamic equations are written in the port-Hamiltonian form described in 2, where P and S are equal to 0, and

$$J = \begin{bmatrix} \mathbf{0} & \boldsymbol{\phi} \\ -\boldsymbol{\phi}^T & \mathbf{0} \end{bmatrix}, R = \begin{bmatrix} R_f & \mathbf{0} \\ \mathbf{0} & \mathbf{0} \end{bmatrix}, g = \begin{bmatrix} \vartheta & -\varphi_\pi \\ \mathbf{0} & -\varphi \end{bmatrix}, M = \begin{bmatrix} \mathbf{0} & \psi \\ -\psi^T & \mathbf{0} \end{bmatrix}$$

This leads to the system described in (48).

Note that $\mathbf{y}_b = -\mathbf{F}_c - \mathbf{F}_c^*$, where $\mathbf{F}_c$ is the set of forces applied by the flow on the contact surface of the mechanical structure. $\mathbf{F}_c^*$ is an extra term that is cancelled in the interconnection between the flow and the mechanical models, as we see in the next section.

5. Fluid-structure model

In this section, we present the interconnection between the fluid and the structure models. From Sections 3 and 4 we have that the total energy of the fluid-structure system is given by

$$H = H_s + H_f \tag{70}$$

where H_s and H_f are defined in (7) and (47) respectively.

Proposition 6. *Let the structure and flow port-Hamiltonian models be described as in Propositions 1 and 5, respectively. Then, the PHS that describes the FSI between these two susbsystems is given by*

$$\begin{bmatrix} \dot{\mathbf{q}}_s \\ \dot{\mathbf{p}}_s \\ \dot{\mathbf{p}}_z \\ \dot{\mathbf{r}} \end{bmatrix} = \begin{bmatrix} \mathbf{0} & I & \mathbf{0} & \mathbf{0} \\ -I & -R_s & C^T\varphi_\pi^T & C^T\varphi^T \\ \mathbf{0} & -\varphi_\pi C & -R_f & \boldsymbol{\phi} \\ \mathbf{0} & -\varphi C & -\boldsymbol{\phi}^T & \mathbf{0} \end{bmatrix} \begin{bmatrix} \partial_{\mathbf{q}_s} H \\ \partial_{\mathbf{p}_s} H \\ \partial_{\mathbf{p}_z} H \\ \partial_{\mathbf{r}} H \end{bmatrix} + \begin{bmatrix} \mathbf{0} & \mathbf{0} \\ C^T\psi^T & I \\ \vartheta & \mathbf{0} \\ \mathbf{0} & \mathbf{0} \end{bmatrix} \begin{bmatrix} \mathbf{u}_p \\ \mathbf{u}_e \end{bmatrix} \tag{71}$$

$$\begin{bmatrix} \mathbf{y}_Q \\ \mathbf{y}_v \end{bmatrix} = \begin{bmatrix} \mathbf{0} & \psi C & \vartheta^T & \mathbf{0} \\ \mathbf{0} & I & \mathbf{0} & \mathbf{0} \end{bmatrix} \begin{bmatrix} \partial_{\mathbf{q}_s} H \\ \partial_{\mathbf{p}_s} H \\ \partial_{\mathbf{p}_z} H \\ \partial_{\mathbf{r}} H \end{bmatrix} \tag{72}$$

where $\mathbf{u}_e$ and $\mathbf{y}_v$ are the external forces and velocities sets of masses of the mechanical submodel, $\mathbf{u}_p$ and $\mathbf{y}_Q$ are the pressure and flow sets in the inlet and outlet boundaries of the fluid submodel, H is the total energy defined in (56), and matrix C describes the interconnection between the mechanical structure and the corresponding flow sections of the fluid model.

Proof. Note that the power exchange between the fluid and mechanical system is given by $\mathbf{u}_b^T \mathbf{F}_c$. Similarly, the power source of the mechanical structure is given by $\mathbf{u}_s^T \mathbf{y}_s$. We consider that $\mathbf{u}_s = f(\mathbf{F}_c) + \mathbf{u}_e$ and $\mathbf{y}_b = -\mathbf{F}_c - \mathbf{F}_c^*$ where $f(\cdot)$ is a linear function and $\mathbf{u}_e$ is the set of external forces applied on the mechanical model. Then, there exists a matrix

C such that $C : \mathbf{y}_s \to \mathbf{u}_b$ and $-C^T : \mathbf{y}_b \to \mathbf{u}_s$. Thus, the fluid-structure model is obtained using the following power preserving interconnection:

$$\begin{bmatrix} \mathbf{u}_s \\ \mathbf{u}_b \\ -\mathbf{y}_v \end{bmatrix} = \begin{bmatrix} \mathbf{0} & -C^T & I \\ C & \mathbf{0} & \mathbf{0} \\ -I & \mathbf{0} & \mathbf{0} \end{bmatrix} \begin{bmatrix} \mathbf{y}_s \\ \mathbf{y}_b + \mathbf{F}_c^* \\ \mathbf{u}_e \end{bmatrix}, \tag{73}$$

obtaining the following set of ODEs:

$$\dot{\mathbf{q}}_s = \partial_{\mathbf{p}_s} H_s \tag{74}$$

$$\dot{\mathbf{p}}_s = -\partial_{\mathbf{q}_s} H_s - R_s \partial_{\mathbf{p}_s} H_s + C^T \left(\varphi_\pi^T \partial_{\mathbf{p}_z} H_f + \varphi^T \partial_{\mathbf{r}} H_f \right) - C^T \mathbf{F}_c^* + C^T \psi^T \mathbf{u}_p + \mathbf{u}_e \tag{75}$$

$$\dot{\mathbf{p}}_z = -\varphi_\pi C \partial_{\mathbf{p}_s} H_s - R_f \partial_{\mathbf{p}_z} H_f + \boldsymbol{\phi} \partial_{\mathbf{r}} H_f + \vartheta \mathbf{u}_p \tag{76}$$

$$\mathbf{r} = -\varphi C \partial_{\mathbf{p}_s} H_s - \boldsymbol{\phi}^T \partial_{\mathbf{p}_z} H_f \tag{77}$$

Additionally, from the interconnection rule in (58), $\mathbf{u}_b = C\mathbf{y}_s$. This implies that the set $\mathbf{q}_f$ of heights of flow sections is given by $\mathbf{q}_f = C\mathbf{q}_s + \mathbf{q}_0$ where $\mathbf{q}_0$ is the set of heights when the flow velocity and pressure are equal to 0. Now, for the i-th height we obtain that

$$\partial_{q_i} K_f = \sum_{j=i-i}^{i+1} \frac{1}{2} \left(\frac{\pi_{zj}}{\rho_0 V_j} \right)^2 \partial_{q_i} V_j = A_{ci} \frac{1}{2} \left(\frac{\pi_{zi}}{\rho_0 V_i} \right)^2 + A_{ni} p_{di}^{\rho} + A_{n(i-1)} p_{d(i-1)}^{\rho}$$

Defining $\mathbf{F}_c^* = \partial_{\mathbf{q}} K_f$, then, $\partial_{\mathbf{q}} K_f = C^T \partial_{\mathbf{q}} K_f = C^T \mathbf{F}_c^*$. Thus, the dynamics of the structure momenta can be rewritten as follows

$$\dot{\mathbf{p}}_s = \underbrace{-\partial_{\mathbf{q}_s} H_s}_{\text{springforces}} \underbrace{- R_s \partial_{\mathbf{p}_s} H_s}_{\text{damping}} + \underbrace{\mathbf{u}_e}_{\text{externalforces}} \underbrace{\overbrace{-\partial_{\mathbf{q}_s} K_f}^{C^T \mathbf{F}_c^*} + C^T \overbrace{\left(\varphi_\pi^T \partial_{\mathbf{p}_z} H_f + \varphi^T \partial_{\mathbf{r}} H_f + \psi^T \mathbf{u}_p \right)}^{-\mathbf{y}_b = \mathbf{F} + \mathbf{F}_c^*}}_{\text{fluidforceoncontactsurfaces:} C^T \mathbf{F}_c} \tag{78}$$

Finally, the system in (57) is obtained by expressing (59), (61), (62) and (63) in the port-Hamiltonian form (4), where P, S and M are equal to zero and

$$R = \begin{bmatrix} \mathbf{0} & \mathbf{0} & \mathbf{0} & \mathbf{0} \\ \mathbf{0} & R_s & \mathbf{0} & \mathbf{0} \\ \mathbf{0} & \mathbf{0} & R_f & \mathbf{0} \\ \mathbf{0} & \mathbf{0} & \mathbf{0} & \mathbf{0} \end{bmatrix} g = \begin{bmatrix} \mathbf{0} & \mathbf{0} \\ C^T \psi^T & I \\ \vartheta & \mathbf{0} \\ \mathbf{0} & \mathbf{0} \end{bmatrix} J = \begin{bmatrix} \mathbf{0} & I & \mathbf{0} & \mathbf{0} \\ -I & \mathbf{0} & C^T \varphi_\pi^T & C^T \varphi^T \\ \mathbf{0} & -\varphi_\pi C & \mathbf{0} & \boldsymbol{\phi} \\ \mathbf{0} & -\varphi C & -\boldsymbol{\phi}^T & \mathbf{0} \end{bmatrix}$$

Note that, the term $\partial_{\mathbf{q}} K_f$ appears as a consequence of the fluid-structure interaction. This term compensates the additional force $\mathbf{F}_c^*$ in the output $\mathbf{y}_b$ of the flow model, as shown in (78). Thus, the power exchange of the FSI is given by $\mathbf{y}_s^T C^T \mathbf{F}_c = \mathbf{u}_b^T \mathbf{F}_c$.

6. Numerical examples

In this section, we present numerical simulations of the proposed port-Hamiltonian FSI model. First, we study a simple system to analyse the pressure behaviour in a node. Later we study a flexible vessel to compare the results obtained with those presented in the literature.

6.1. A simple FSI system

[t][Simple Fluid-Structure system] [t][Relative variation of the density] [b][Pressures in the node] [b][Position of masses]

Consider a tube with two fluid sections with moving boundaries and one node. The upper boundary of each section is coupled with a mass-spring damper system, as shown in Figure 4(a). The corresponding fluid-structure port-Hamiltonian model proposed in Section 5, for this example, has the following state variables $\mathbf{q}_s = [\bar{q}_1 \bar{q}_2]^T$, $\mathbf{p}_s = [\pi_1 \pi_2]^T$, $\mathbf{p}_z = [\pi_{z1} \pi_{z2}]^T$ and $\mathbf{r} = \rho_1$. The interconnection, dissipation and input sub-matrices for the model (57) are given by

$$C^T \varphi_\pi^T = \begin{bmatrix} \frac{A_{c1}\pi_{z1}}{V_1} & 0 \\ 0 & \frac{A_{c2}\pi_{z2}}{q_2} \end{bmatrix}, \phi = \begin{bmatrix} -A_1 \frac{\rho_1^2}{\kappa} \\ A_2 \frac{\rho_1^2}{\kappa} \end{bmatrix}, C^T \varphi = \begin{bmatrix} \frac{\rho_1^2}{\kappa}\left(\frac{A_{c1}}{2} + A_{n1}\right) \\ \frac{\rho_1^2}{\kappa}\left(\frac{A_{c2}}{2} + A_{n1}\right) \end{bmatrix}, C^T \psi^T = \begin{bmatrix} \frac{A_{c1}}{2} & 0 \\ 0 & \frac{A_{c2}}{2} \end{bmatrix}$$

$$\vartheta = \begin{bmatrix} A_1 & 0 \\ 0 & -A_2 \end{bmatrix}, R_s = \begin{bmatrix} d_1 & 0 \\ 0 & d_2 \end{bmatrix}, R_f = \begin{bmatrix} r_1 & 0 \\ 0 & r_2 \end{bmatrix}$$

and the energy gradient is given by $\partial_{\mathbf{q}_s} H = \begin{bmatrix} F_{s1} + A_{c1}\frac{\rho_0}{2}v_1^2 + A_{n1}p_{d1}0.2pt \\ F_{s2} + A_{c2}\frac{\rho_0}{2}v_2^2 + A_{n1}p_{d1} \end{bmatrix}$, $\partial_{\mathbf{p}_s} H = \begin{bmatrix} \pi_1/m_1 \\ \pi_2/m_2 \end{bmatrix}$, $\partial_{\mathbf{p}_z} H = \begin{bmatrix} \pi_{z1}/\rho_0 V_1 \\ \pi_{z2}/\rho_0 V_2 \end{bmatrix}$ and $\partial_{\mathbf{r}} H = \frac{\kappa}{\rho_1^2}(p_1 + p_{d1})$.

We consider the following parameters for this system: $k_1 = 100\text{N/m}$, $k_2 = 75\text{N/m}$, $k_c = 100\text{N/m}$, $m_1 = m_2 = 0.005\text{kg}$, $d_1 = d_2 = 0.025\text{Ns/m}$ $\rho_0 = 1.1376\text{kg/m}^3$, $\kappa = 10^{-10}\text{kg}$, $\beta_S = 142 \times 10^3\text{Pa}$, $L = 0.01\text{m}$, $\ell_1^* = \ell_2^* = 0.01\text{m}$ and $q_{10} = q_{20} = 5 \times 10^{-3}\text{m}$. Figure 4(b–d) show the simulation results for the relative variation of density $\Delta\rho_1 = 100\frac{\rho_1 - \rho_0}{\rho_0}$, pressures in the node and motion of masses, respectively, when the external inlet and outlet total pressures are fixed to $P_i = 800\text{Pa}$ $t \geq 0$ and $P_i = 0\text{Pa}$ otherwise, and $P_o = 0\text{Pa}$ t. Note that $\Delta\rho_1 \leq 0.1\%$, this variation is small enough to be neglected in typical incompressible assumptions. However, it is useful in this work to describe the pressure and the coupling between two incompressible sections. Moreover, this small variation implies a small static pressure p_1^ρ, such that, the behaviour of the total pressure P_1^ρ in the node is governed by the dynamic pressure p_{d1}^ρ, as shown in Figure 4(c). The motion of the masses shows an oscillatory behaviour and tends to settle in a new equilibrium point according to the pressure distribution in the fluid.

6.2. Flexible vessel

A flexible Vessel is a benchmark problem used to analyse the pressure impulse propagation in an FSI system. It is related to the blood flow through an artery and it

has been used for validating the performance of FSI solvers [2,3,13]. Considering an axisymmetric vessel behaviour, we can approximate the vessel structure and fluid using the model proposed in this paper with equal number of masses and incompressible fluid sections, i.e. $n = N$. The structure parameters are approximated using the following formula

$$\ell_i^* = L_s/N, \quad iq_{0i} = r_s, \quad im_i = 2\rho_s r_s h_s \ell_i^*, \quad i$$

$$k_i = \beta_1 \lambda_m \frac{\ell_i^* h_s}{r_s}, \quad ik_{ci} = \beta_2 \mu_m \frac{r_s h_s}{\ell_i^*}, \quad id_i = \zeta \sqrt{m_i k_i}, \quad i$$

where r_s and L_s are the vessel radius and length, respectively, ρ_s and h_s are the density and thickness of the vessel wall (as shown in Figure 6), λ_m and μ_m are the Lamé coefficients, and β_1 and β_2 are dimensionless factors. The damping parameters are empirically adjusted. For the fluid we consider $A_i = r_s q_i$, $V_i^* = A_i \ell_i^*$ and $\kappa = \rho_0 V_i^* 10^{-3}$.

First, we use the parameters proposed in Section 5.1 of [13] where $L_s = 0.05$m, $h_s = 0.001$m, $\rho_s = 1.2 \times 10^3$kg/m^3, $\lambda_m = 17.308 \times 10^4$Pa, $\mu_m = 11.538 \times 10^4$Pa, and $\rho_0 = 1 \times 10^3$kg/m^3. We divide the structure into two different numbers of sections, $N = 51$ and $N = 71$, and equal numbers of incompressible sections in the fluid, i.e. matrix C in (58) is the identity matrix. We use $\beta_1 = 6.7$, $\beta_2 = 1.5 \times 10^{-5}$, and $\zeta = 0.4$. The parameter values are summarized in Table 1. Using the same input conditions as described in [13], i.e. $P_o = 0$Pa, t and

$$P_i = \begin{pmatrix} 1.333 \times 10^3\text{Pa}, & 0 \le t \le 3 \times 10^{-3}\text{s} \\ 0\text{Pa}, & \text{otherwise} \end{pmatrix}$$

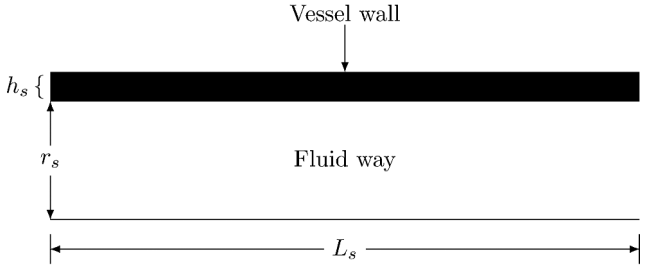

Figure 6. Flexible vessel description.

Table 1. Simulation parameters for the flexible vessel problem.

Using the material parameters proposed in et~al.(2019)Lozovskiy,		
2*N = 51	1*Structure	$k_i = 73.9483$N/m, $k_{ci} = 2.7 \times 10^{-2}$N/m, $d_i = 0.0209$Ns/m $\quad i$, $d_{ci} = 0 \quad i$, $m_i = 3.7 \times 10^{-5}$kg
	1*Fluid	$\rho_0 = 1 \times 10^3$kg/m^3, $\beta_S = 2.15 \times 10^9$Pa, $\kappa = 7.7 \times 10^{-8}$kg, $\ell_i^* = 9.8 \times 10^{-4}$m
2*N = 71	1*Structure	$k_i = 51.9883$N/m, $k_{ci} = 3.86 \times 10^{-2}$N/m, $d_i = 0.0148$Ns/m $\quad i$, $d_{ci} = 0 \quad i$, $m_i = 2.65 \times 10^{-5}$kg
	1*Fluid	$\rho_0 = 1 \times 10^3$kg/m^3, $\beta_S = 2.15 \times 10^9$Pa, $\kappa = 5.53 \times 10^{-8}$kg, $\ell_i^* = 7.04 \times 10^{-4}$m
Using the material parameter proposed in À		
2*N = 71	1*Structure	$k_i = 100.604$N/m, $k_{ci} = 0.9085$N/m, $d_i = 0.0434$Ns/m, $\quad i$, $d_{ci} = 0, \quad i$, $m_i = 2.92\times^{-5}$kg
	1*Fluid	$\rho_0 = 1 \times 10^3$kg/m^3, $\beta_S = 2.15 \times 10^9$Pa, $\kappa = 6.63 \times 10^{-8}$kg, $\ell_i^* = 8.45 \times 10^{-4}$m

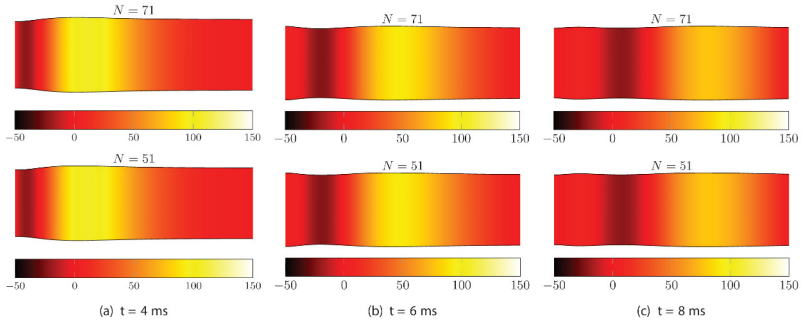

Figure 7. Static pressure (Pa) distribution, $\mathbf{p}_1^{\rho}$, along the tube and scaled structure displacements for different time instants and two different number of sections.

with a sample time of 4×10^{-5}s, we obtain the pressure wave propagation shown in Figure 7, where the structure displacements have been scaled 10 times for the sake of clarity. Note that the speed propagation and attenuation of the pressure waves are in correspondence with the results in [13, Figure 2]. However, a difference from the results in [13] is the static pressure undershoot behind the pressure pulse propagation and a negative displacement of the tube walls. Note that the distance between this undershoot and the pressure pulse increases as the pulse propagates through the tube. This behaviour is consistent with the results reported in [32, Figure 6], Figure 6, where a 3D model of the flexible tube is studied. Regarding the negative displacement, consider the displacement at half length of the structure shown in Figure 8. This displacement shows the same pattern as the radial displacement reported in [13, Figure 3b]. Then, the main difference with respect to the results reported in [13] is given by the displacement at both ends of the tube. This is due to the fact that in [13] the tube is fixed at both ends, restricting the motion of the tube near these locations. In this work we do not implement this restriction, allowing greater displacement at the ends of the tube, as shown in Figure 7(a).

Now, we consider the parameters used in [3] where $L_s = 0.06$m, $h_s = 0.001$m, $\rho_s = 1.1 \times 10^3$kg/m^3, $\lambda_m = 17 \times 10^4$Pa, $\mu_m = 5.75 \times 10^4$Pa, and $\rho_0 = 1 \times 10^3$kg/m^3. The parameters are obtained using $N = 71$, $\beta_1 = 1.1$, $\beta_2 = 8.5 \times 10^{-5}$ and $\zeta = 0.8$ (see

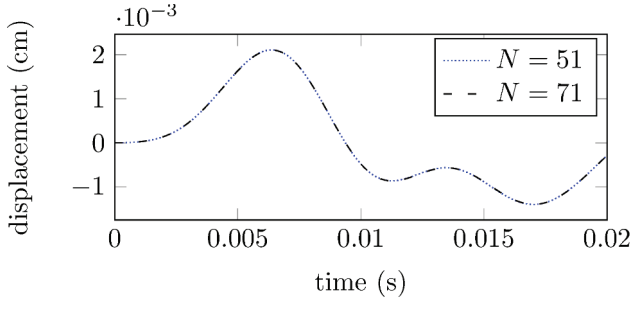

Figure 8. Displacement of the wall in the half-length point of the structure (Displacements $\bar{q}_{26}$ and $\bar{q}_{36}$ for $N = 51$ and $N = 71$, respectively).

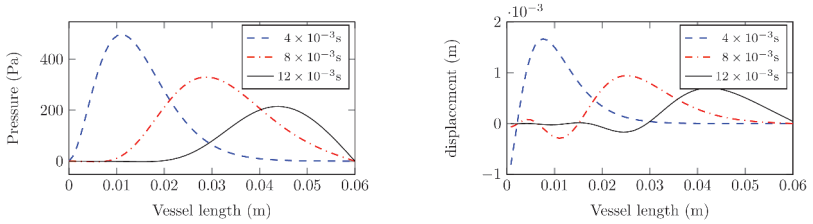

(a) Pressure distribution in the flow (b) Wall displacement

Figure 9. Simulation results for flexible vessel using the material parameter of [2] at instants 4×10^{-3}s, 8×10^{-3}s and 12×10^{-3}s. (a) Static pressure distribution, $\mathbf{p}_1^{\rho}$, along the tube. (b) Wall displacement distribution, $\mathbf{q}_s$, along the tube.

Table 1 for details). We define the input pressure pulse similarly as in [2,3], i.e. $P_o = 0$Pa and

$$P_i = \begin{cases} 666.5\left(1 - \cos\left(\frac{6.28t}{0.003}\right)\right)\text{Pa}, & 0 \leq t \leq 0.003\text{s} \\ 0\text{Pa}, & \text{otherwise} \end{cases}$$

Figure 9 shows the pressure distribution and structure displacement for three different time instants. The pressure distributions shown in Figure 9.a at time instants 4×10^{-3}s, 8×10^{-3}s and 12×10^{-3}s are in correspondence with the results reported in [2, Figure 8] and [3, Figure 8] at $h = 0.01$. Similarly, the shape of the wall displacements shown in Figure 9(b) is consistent with the results reported for the fluid–structure interface displacement in [2, Figure 9] and [3, Figure 7] at $h = 0.01$. However, a difference between our results and those shown in [2,3] is given by the negative displacement at the left-end side of the tube in the first instants of the simulation. As we have commented above, this difference is due to the fact we do not constraint the motion at the ends of the tube, allowing a free motion of the wall.

7. Conclusion

A scalable approach for the modelling of 1D incompressible fluid interactions with flexible structures has been proposed. Describing the mechanical structure by sets of mass-spring-damper systems and relaxing the incompressibility hypothesis a simple and scalable coupled fluid-mechanical port-Hamiltonian model has been derived. The fluid and the mechanical structure are coupled through a power-preserving interconnection between the velocities and forces in the contact areas of the two systems. Instrumental for the construction of the model is the definition of compressible nodes which allow the total pressure coupling between incompressible fluid sections. Numerical results show that the density variations in the nodes are sufficiently small to consider the fluid incompressible. A flexible vessel model has been studied and the results obtained show pressure wave propagation in the flow and a structure motion in correspondence with previous works based on finite-element models. Since the proposed model is a port-Hamiltonian system it can be exploited for control purposes or to interconnect with other fluid-mechanical systems.

Acknowledgments

This work is supported by the European Commission Marie Sklodowska-Curie Fellowship, ConFlex ITN Network and by the INFIDHEM project under the reference codes 765579 and ANR-16-CE92-0028, respectively, also by CONICYT through grands CONICYT-PFCHA/Bec. Doc. Nac./2017-21170472, FONDECYT 1181090, FONDECYT 1191544 and BASAL FB0008, and UTFSM PIIC scholarship 013/2018.

Disclosure statement

No potential conflict of interest was reported by the authors.

Funding

This work was supported by the Agence Nationale de la Recherche [INFIDHEM ANR-16-CE92-0028]; Comisión Nacional de Investigación Científica y Tecnológica [CONICYT-PFCHA/Bec. Doc. Nac./2017-21170472, FONDECYT 1181090, FONDECYT 1191544, and FB0008]; H2020 Marie Skłodowska-Curie Actions [ConFlex ITN Network 765579]; Universidad Técnica Federico Santa María [UTFSM PIIC scholarship 013/2018]; EIPHI Graduate School [contract ANR-17-EURE-0002].

ORCID

Luis A. Mora http://orcid.org/0000-0002-2112-6847

References

[1] H.-J. Bungartz and M. Schäfer (eds.), *Fluid-Structure Interaction*, Lecture Notes in Computational Scienceand Engineering Vol. 53, Springer Berlin Heidelberg, Berlin/Heidelberg, 2006. doi:10.1007/3-540-34596-5

[2] M. Bukač, S. Čanić, R. Glowinski, B. Muha, and A. Quaini, *A modular, operator-splitting scheme for fluid-structure interaction problems with thick structures*, Int. J. Numer. Methods Fluids. 74 (8) (2014), pp. 577–604. doi: 10.1002/fld.3863

[3] M. Bukač, S. Čanić, and B. Muha, *A partitioned scheme for fluid-composite structure interaction problems*, J Comput Phys. 281 (2015), pp. 493–517. doi:10.1016/j.jcp.2014.10.045

[4] A.R. Ghigo, J-M.. Fullana, and P-Y.. Lagrée, *A 2D nonlinear multiring model for blood flow in large elastic arteries*, J Comput Phys. 350 (2017), pp. 136–165. doi: 10.1016/j.jcp.2017.08.039

[5] F. Chouly, A. Van Hirtum, P.-Y. Lagrée, X. Pelorson, and Y. Payan, *Numerical and experimental study of expiratory flow in the case of major upper airway obstructions with fluid-structure interaction*, J Fluids Struct. 24 (2) (2008), pp. 250–269. doi:10.1016/j.jfluidstructs.2007.08.004

[6] M.R. Rasani, K. Inthavong and J.Y. Tu, *Three-Dimensional Fluid-Structure Interaction Modeling of Expiratory Flow in thePharyngeal Airway*, in 5th Kuala Lumpur International Conference on Biomedical Engineering 2011 IFMBE Proceedings, N.A.A. Osman, W.A.B. W. Abas, A.K.A. Wahab and H. Ting, eds., Springer -Verlag Berlin Heidelberg, Berlin, 2011, pp. 467–471

[7] S.L. Thomson, L. Mongeau, and S.H. Frankel, *Aerodynamic transfer of energy to the vocal folds*, J. Acoust. Soc. Am. 118 (3) (2005), pp. 1689–1700. doi:10.1121/1.2000787

[8] P. Šidlof, J. Horáček, and V. Řidký, *Parallel CFD simulation of flow in a 3D model of vibrating human vocal folds*, Comput Fluids 80 (2013), pp. 290–300. doi:10.1016/j.compfluid.2012.02.005

[9] W. Jiang, X. Zheng, and Q. Xue. *Computational modeling of fluid-structure-acoustics interaction during voice production*, Front. Bioeng. Biotechnol. 5 (2017) doi: 10.3389/fbioe.2017.00007

[10] J. Donea, A. Huerta, J.-P. Ponthot, and A. Rodríguez-Ferran, *Arbitrary Lagrangian-Eulerian methods*, in *Encyclopedia of Computational Mechanics* Vol. 1, E. Stein, R. de Borst and T.J.R. Hughes, eds., John Wiley & Sons, Ltd, Chichester, UK, 2004. doi:10.1002/0470091355.ecm009

[11] K.K.L. Wong, P. Thavornpattanapong, S.C.P. Cheung, and J. Tu, *Numerical stability of partitioned approach in fluid-structure interaction for a deformable thin-walled vessel*, Comput Math Methods Med 2013 (2013), pp. 1–10. doi:10.1155/2013/638519.

[12] P. Causin, J.F. Gerbeau, and F. Nobile, *Added-mass effect in the design of partitioned algorithms for fluid-structure problems*, Comput Methods Appl Mech Eng 194 (42-44) (2005), pp. 4506–4527. doi: 10.1016/j.cma.2004.12.005

[13] A. Lozovskiy, M.A. Olshanskii, and Y.V. Vassilevski, *Analysis and assessment of a monolithic FSI finite element method*, Comput Fluids 179 (2019), pp. 277–288. doi:10.1016/j.compfluid.2018.11.004

[14] G. Papadakis, *Coupling 3D and 1D fluid-structure-interaction models for wave propagation in flexible vessels using a finite volume pressure-correction scheme*, Commun. Numer. Methods Eng. 25 (5) (2009), pp. 533–551. doi: 10.1002/cnm.1212.

[15] V. John, *Finite Element Methods for Incompressible Flow Problems*, Springer Series in Computational Mathematics Vol. 51, Springer International Publishing, Cham, 2016. doi:10.1007/978-3-319-45750-5

[16] L.A. Mora, H. Ramírez, J.I. Yuz, and Y.L. Gorrec, *A scalable port-hamiltonian model for incompressible fluids in irregular geometries*, IFAC-PapersOnLine 52 (2019), pp. 102–107. doi:10.1016/j.ifacol.2019.08.018.

[17] A. van der Schaft and B. Maschke, *Hamiltonian formulation of distributed-parameter systems with boundary energy flow*, J. Geom. Phys 42 (1-2) (2002), pp. 166–194. doi:10.1016/S0393-0440(01)00083-3

[18] P. Kotyczka, *Discretized models for networks of distributed parameter port-Hamiltonian systems*, Proceedings of the 8th International Workshop on Multidimensional Systems (nDS13), VDE, Erlangen, Germany, pp. 63–67 2013.

[19] R. Altmann and P. Schulze, *A port-Hamiltonian formulation of the Navier-Stokes equations for reactive flows*, Syst Control Lett 100 (2017), pp. 51–55. doi:10.1016/j.sysconle.2016.12.005.

[20] Siuka, M. Sch, and K. Schlacher, *Hamiltonian evolution equations of inductionless magnetohydrodynamics*, Proceedings of the 19th International Symposium on Mathematical Theory of Networks and Systems (MTNS 2010), BUdapest, Hungary, pp. 1889–1896, 2010.

[21] F.L. Cardoso-Ribeiro, D. Matignon, and V. Pommier-Budinger, *A port-Hamiltonian model of liquid sloshing in moving containers and application to a fluid-structure system*, Fluids Struct 69 (2017), pp. 402–427. doi:10.1016/j.jfluidstructs.2016.12.007.

[22] V. Duindam, A. Macchelli, S. Stramigioli, and H. Bruyninckx, *Modeling and Control of Complex Physical Systems*, Springer Berlin Heidelberg, Berlin, 2009. doi: 10.1007/978-3-642-03196-0

[23] A. van der Schaft and D. Jeltsema, *Port-Hamiltonian Systems Theory: An Introductory Overview*, Now Publishers, Boston, MA, USA, 2014. doi:10.1561/9781601987877

[24] Peter J. Olver, *Applications of Lie Groups to Differential Equations*, Graduate Texts in Mathematics Vol. 107, F.W. Gehring, P.R. Halmos and C.C. Moore, eds., Springer US, New York, 1986. doi:10.1007/978-1-4684-0274-2

[25] R.B. Bird, W.E. Stewart, E.N. Lightfoot, and D.J. Klingenberg, *Introductory Transport Phenomena*, John Wiley & Sons, Inc, USA, 2015.

[26] P. M. Gresho and R. L. Sani, *Incompressible Flow and the Finite Element Method, Volume 1: Advection-Diffusion and Isothermal Laminar Flow*, John Wiley & Sons, Inc, New York, USA, 1998.
[27] R.L. Panton, *Incompressible Flow*, 4th ed., John Wiley & Sons, Inc, New Jersey, USA, 2013. doi:10.1002/9781118713075
[28] R. Mulley, *Flow of Industrial Fluids: Theory and Equations*, CRC Press, USA, 2004. doi: 10.1201/9781420038286
[29] J. Pérez-García, E. Sanmiguel-Rojas, and A. Viedma, *New coefficient to characterize energy losses in compressible flow at T-junctions*, Appl Math Model 34 (12) (2010), pp. 4289–4305. doi: 10.1016/j.apm.2010.05.005.
[30] R. Brodkey and H. Hershey, *Transport Phenomena: A Unified Approach*, Chemical Engineering Series, McGraw Hill International, New York, 1988.
[31] J. W. Murdock, *Fundamental Fluid Mechanics for the Practicing Engineer*, Dekker Mechanical Engineering Series Vol. 8, CRC Pres, New York, 2018. doi: 10.1201/9781315274065
[32] J. Degroote, R. Haelterman, S. Annerel, P. Bruggeman, and J. Vierendeels, *Performance of partitioned procedures in fluid-structure interaction*, Comput Struct 88 (7-8) (2010), pp. 446–457. doi: 10.1016/j.compstruc.2009.12.006.

Appendix

Notation Table

General notation			
Symbol	Description	Symbol	Description
$\mathbf{0}$	Zero matrix of appropriate dimensions	I	Identity matrix of appropriate dimensions
∇f	Gradient of f	$\nabla \cdot (f)$	Divergence of f
$\nabla^2 f$	Laplacian of f	∂_t	Partial derivative with respect to time
∂_x	Partial derivative with respect to x	$\dot{x}$	Time derivative of x
N_s	Number of structure sections	N	Number of incompressible flow sections
Structure sub-system			
Symbol	Description	Symbol	Description
m_i, π_i	Mass and momentum of the i-th structure section	k_i, d_i	Spring and damper coefficients in the i-th structure section
k_{ci}, d_{ci}	i-th coupling spring and damper coefficients	$\bar{q}_i$	Displacement of i-th structure section
$\mathbf{p}_s$	Set of structure momenta	$\bar{q}_s$	Set of structure displacement
v_{ci}	Velocity of the i-th structure section.	H_s	Total energy of the structure

Fluid sub-systemA_{ci}Fluid-structure contact area in the i-thv_iAverage longitudinal velocity in the i-thincompressible flow sectionincompressible flow sectionλ_iLoss factor of the i-th incompressible flowV_iVolume of the i-th incompressible flowsectionsectionA_{nj}Fluid-structure contact area in the j-th node$\bar{V}_j$Volume of the j-th nodeρ_0Reference fluid densityρ_jDensity in the j-th nodep_j^ρ, p_{dj}^ρStatic and dynamic pressures in the j-th nodeπ_{zi}Average momentum of the i-th incompressible flow section$\mathbf{p}_z$Set of fluid momentarSet of node densitiesβ_SBulk modulus of the fluidκMass of nodesP_iTotal pressure in the inlet fluid boundaryP_oTotal pressure in the outlet fluid boundaryQ_iFlow in the inlet fluid boundaryQ_oFlow in the outlet fluid boundary